# THE EUROPEAN PHYSICAL JOURNAL PLUS

#### Regular Article



# Structural, magnetic, and critical behavior of CrTe<sub>1-x</sub>Sb<sub>x</sub> alloys

M. Kh. Hamad<sup>1,a</sup>, Yazan Maswadeh<sup>2</sup>, E. Martinez-Teran<sup>3</sup>, A. A. El-Gendy<sup>3,b</sup>, Kh. A. Ziq<sup>1,c</sup>

Department of Physics, King Fahd University of Petroleum and Minerals, Dhahran 31261, Saudi Arabia

Received: 12 February 2021 / Accepted: 5 May 2021 © The Author(s), under exclusive licence to Società Italiana di Fisica and Springer-Verlag GmbH Germany, part of Springer Nature 2021

**Abstract** We investigate the structural and critical properties of  $CrTe_{1-x}Sb_x$  with  $0.0 \le x \le 0.2$ . The XRD patterns revealed that Sb substitution resulted in a pure NiAs-hexagonal structure with P6<sub>3</sub>/mmc (194) space group. Lattice refinement of the structure revealed little changes in the *a*-lattice parameter, along with a more pronounced reduction in the *c-axis*. The critical behavior in  $CrTe_{1-x}Sb_x$  has been investigated using the magnetization isotherms near the ferromagnetic transition. The obtained critical exponents  $(\beta, \gamma, \text{ and } \delta)$  revealed that all samples (with  $0.0 \le x \le 0.2$ ) closely follow a mean field-like behavior with ferromagnetic Curie temperature near room temperature. The results from Widom scaling relation indicate self-consistency of the acquired values. Moreover, the magnetization isotherms near the Curie temperature follow a universal scaling behavior, giving further support for the obtained critical exponents.

#### 1 Introduction

Cr-based pnictogens and chalcogens continue to attract the attention of scientists due to their versatile physical properties [1-5]. These properties range from superconducting to semiconducting and half-metallic [6, 7], ferromagnetic van der Waals to antiferromagnetic (AFM) behavior [8-14]. Some of the emerging possible applications are in magnetic cooling and spintronic devices [14]. The binary compounds of Cr-pnictogens (N, As, Sb) and the Cr-chalcogens (S, Se, Te) crystalize in the hexagonal NiAs crystal structure [1-5]; however, the chemical bonding may lead to diverse magnetic and physical properties. Ionic bonding dominates the chalcogenides, while the bonding in pnictide is nonionic. For instance,  $Cr_x$ Te is a ferromagnetic (FM) material with a Curie temperature covering wide range (320-360 K) depending on the value of x [6-15]. It is well established that  $Cr_x$ Te is nonstoichiometric and does not occur in pure hexagonal phase [16, 17]. While substitution at the Cr sites helps

Published online: 11 May 2021



<sup>&</sup>lt;sup>2</sup> Department of Physics and Science of Advanced Materials Program, Central Michigan University, Mount Pleasant, MI 48859, USA

<sup>&</sup>lt;sup>3</sup> Department of Physics, The University of Texas at El Paso (UTEP), El Paso, TX 79968, USA

<sup>&</sup>lt;sup>a</sup> e-mail: mhamad@kfupm.edu.sa (corresponding author)

<sup>&</sup>lt;sup>b</sup> e-mail: aelgendy@utep.edu (corresponding author)

<sup>&</sup>lt;sup>c</sup> e-mail: kaziq@kfupm.edu.sa (corresponding author)

516 Page 2 of 14 Eur. Phys. J. Plus (2021) 136:516

to stabilize the hexagonal NiAs structure, deficiency and defects may also stabilize other structures like trigonal  $Cr_2Te_3$  and monoclinic  $Cr_3Te_4$  structure. Chromium antimony CrSb is antiferromagnetic with  $T_N \sim 700$  K, and it crystalizes in a NiAs-type structure [18–22] with  $\mu_{\rm eff} = 3.89 \, \mu_{\rm B}$  [23, 24]. In CrSb, the Cr spins are aligned ferromagnetically within the basal plane; while in the adjacent planes the spins are aligned antiferromagnetically [22]. Substitution in the solid solutions of  $CrTe_{1-x}Sb_x$  affects the spins configurations and the magnetic phase in this compound [21, 25]. Increasing the Sb concentrations in  $CrTe_{1-x}Sb_x$  leads to a gradual reduction in FM ordering temperature and the saturated magnetization along with moderate reduction in unit cell volume. At high concentration of Sb, a more complex magnetic phases may occur such as canted spin structures and noncollinear spin configurations and even spin-glass like behavior have been observed [14, 26, 27]. Some of these magnetic changes qualitatively agree with de Gennes model of the double exchange interaction in AFM–FM system [28].

Preliminary critical behavior analysis in  $CrTe_{1-x}Sb_x$  has been published in an earlier work [29] where we investigate the effect of Sb substitution over relatively wide range. The modified Arrott plots and Kouvel–Fisher critical exponents' analyses revealed that upon increasing the Sb, the critical exponents deviate significantly from the mean field values and gradually shift toward 3D Heisenberg models. More recently, we found that repeated grinding and annealing during sample preparation improve the phase purity in  $CrTe_{1-x}Sb_x$ , especially at low Sb concentration [14]. For these samples, we investigated the magnetocaloric effect near room-temperature  $CrTe_{1-x}Sb_x$  and found that the relative cooling power is comparable to pure Gd—the prototype magnetocaloric material.

In this work, we extend our investigation of the magnetic and the structural properties of  $CrTe_{1-x}Sb_x$  alloys at low Sb concentrations. The samples used in this study are the same samples we used in Ref. 14. We also investigate the detailed properties of the critical behavior near the FM-PM transition in these newly prepared samples and compare them with our earlier woks [29]. We also include evidences on the changes in the bond length and angle with Sb substitution that ultimately may affect the magnetic and critical behavior. This may lead to a better understanding of the observed differences with earlier work on the critical behavior [29] in this material.

#### 2 Experimental techniques

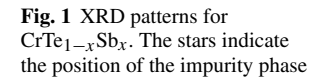
Polycrystalline  $\text{CrTe}_{1-x}\text{Sb}_x$  ( $x \le 0.2$ ) was prepared using high-temperature solid-state reaction [30, 31]. High-purity (4–5 N) powders of Cr, Te, and Sb are used. The detail of the preparation method is reported in our previous work [29]; however, for the samples in this study we used several repetition of intermediate grinding and annealing to improve the phase purity and quality of the samples. Bruker X-ray diffractometer D2-Phaser with Cu K $\alpha$  ( $\lambda$  = 1.54056 Å) has been used to obtain the powdered XRD patterns over 20°–80° [14, 32]. We used Rietveld refinements available in FULLPROF software to analyze the XRD patterns. Quantum design 3-T VersaLab has been used to collect the magnetic data in the temperature range of 50–400 K.

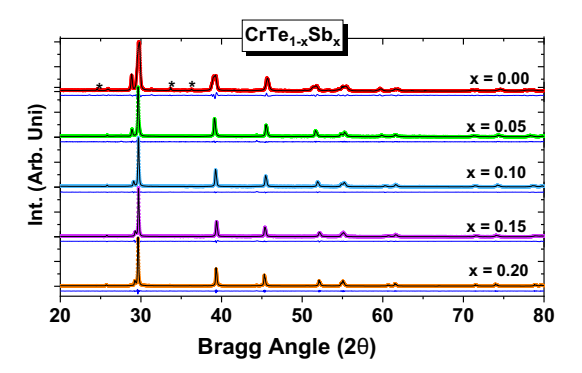
## 3 Analysis and results

Figure 1 shows the room-temperature XRD patterns of the studied  $CrTe_{1-x}Sb_x$  samples. Rietveld refinement of the data was carried out to determine the lattice parameters, phase



Eur. Phys. J. Plus (2021) 136:516 Page 3 of 14 516





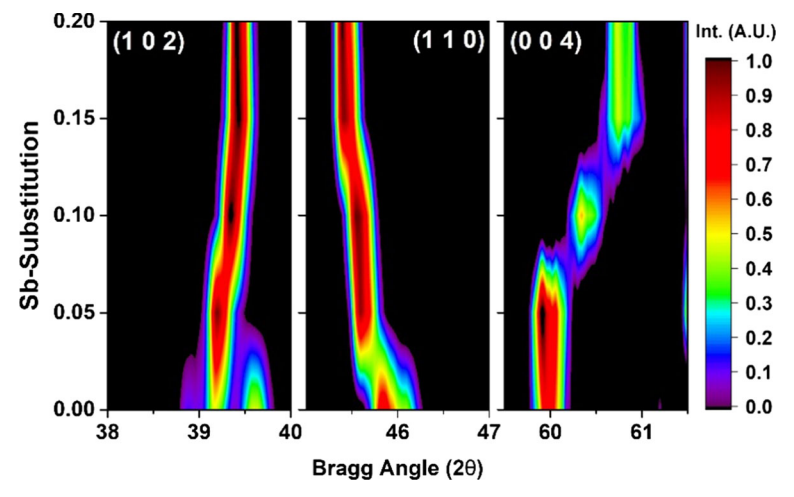


**Fig. 2** A colorful map of selected diffraction peaks with Miller indices shows the changes in peaks position a long with increasing the Sb substitution ratio in the  $CrTe_{1-x}Sb_x$  samples, and the intensity of the peaks increases by going from violet to dark red color. The *y*-axis increases along with the Sb concentration

purity, and structure [33, 34]. The results and the lattice parameters for all investigated samples are discussed in detail elsewhere [14]. Those observations are consistent with the noticed shifts of the positions of the diffractions peaks with the increasing the Sb substitution ration in the samples (Fig. 2); the color map at Fig. 2 shows a noticeable shift in the  $(0\ 0\ l)$  peaks to higher angles indicating a shortening in the *c-lattice* parameter in direct space.

A relatively smaller shift to the left in the ( $h \ k \ \theta$ ) peaks indicates a relaxation along the basal plane a-lattice. Moreover, the figure (for x=0.0) also reveals the presence of secondary-phase  $Cr_2O_3$ , which has a trigonal structure with R-3c space group, leading to the nonstoichiometric  $Cr_x$ Te sample in line with earlier results [8]. Street et al. concluded that chromium telluride  $Cr_x$ Te exists over a range of Te concentration with the hexagonal structure [8, 35]. The Wyckoff positions for the hexagonal structure are given in Table 1. Sb substitution causes relaxation of the atomic bond along (a-b) axes,; this probably will reflect residual stress along the c-axis (Fig. 3) leading to the observed variations in the lattice parameters and the overall increase in the volume of the unit cell for x=0-0.10 [see 14].

The magnetization dependence on temperature in the range of 50–400 K at H = 0.03 T is published elsewhere [14]. The thermomagnetic curves for the selected samples (x = 0.00,



516 Page 4 of 14 Eur. Phys. J. Plus (2021) 136:516

**Table 1** Wyckoff position for  $CrTe_{1-x}Sb_x$  hexagonal structure space group P6<sub>3</sub>/mmc (194)

Atom	Wyckoff	Site	x/a	y/b	z/c
Cr	2a	- 3 m	0	0	0
Te/Sb	2c	- 6m2	1/3	2/3	1/4

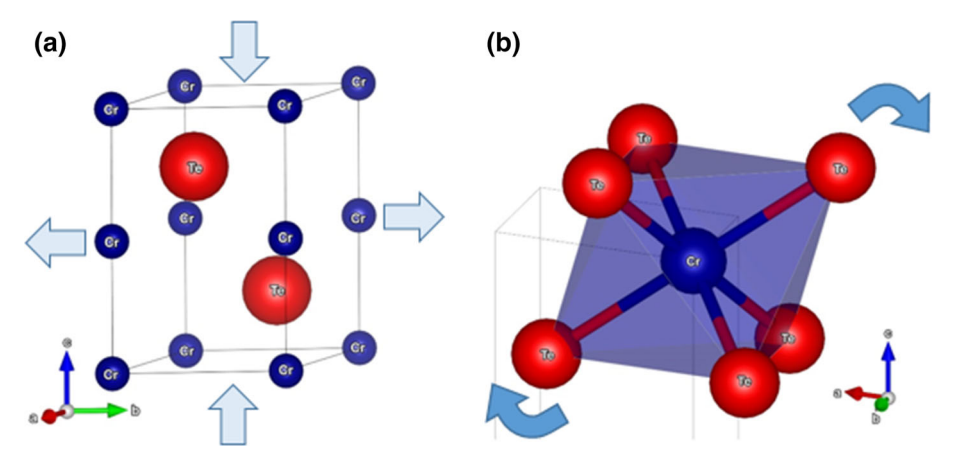


**Fig. 3** Unit cell structure of the CrTe1-xSbx hexagonal phase. The red balls (big) represent Te atoms, while the blue ones (small) represent Cr atoms. The arrows at **a** indicate the changes in the unit cell dimensions by increasing the Sb substitution ratio; **b** shows the CrTe octahedron

0.10, and 0.20) reveal a clear FM–PM phase transition at an inflection points ~ 325.0, 296.0, and 287.0 K, respectively [14]. The results also reveal a slight increase in the magnetization along with sharper transition increasing the concentration of antimony. This probably indicates an increase in the effective magnetic moment per Cr-ion resulting from the exchange interaction with increasing Sb concentration. Figure 4 presents the variations of the inverse magnetic susceptibility ( $\chi^{-1}$ ) with temperature. In the paramagnetic region (i.e., above Tc), the inverse magnetic susceptibility obeys Curie–Weiss law  $\chi = C(T - \theta_p)^{-1}$ , where C and  $\theta_p$  are the Curie constant and the Curie temperature, respectively, following a linear behavior down to  $\theta_p$  in all samples. The linear extrapolation gives the following ( $\theta_p$ ) values 344, 309, and 302 K for x = 0.0, 0.1 and 0.2, respectively [14]. The values of  $\theta_p$  are higher than the Tc values obtained from the inflection points of the M versus T curves. This probably suggests more complex spin configuration than normal FM spin configuration. Recently, Kong et al. observed similar results in CrSbSe<sub>3</sub> [36].

The linear portion of the  $\chi^{-1}$  versus T curves can be used to evaluate the effective magnetic moment  $\mu_{\rm eff}$  using  $\mu_{\rm eff} = \sqrt{3k_BC/N} = \sqrt{8C}\mu_{\rm B}$ , where C is the inverse of the slope and  $\mu_{\rm B}$  is the Bohr magneton. The obtained values are 3.92  $\mu_{\rm B}$ , 4.40 and 4.56 for x=0.0, 0.1 and 0.2, respectively. The expected value for  ${\rm Cr^{3+}}$  is 3.87  $\mu_{\rm B}$  [23, 24]. These values indicate a gradual increase in the Cr effective moment with increasing Sb concentration. These values are in line with the noticed increase in the observed magnetization seen in [14]. The obtained values of  $\mu_{\rm eff}$  along with  $\theta_{\rm B}$  are listed in Table 2.

The magnetic isotherms M(H, T) of CrTe sample are shown in Fig. 5 in the temperature range of 300–376 K. The magnetic behavior in Fig. 5 is deeply discussed elsewhere [14]. The magnetization data in Fig. 5 are presented in modified Arrott plots (MAP) in Fig. 6 in order



Eur. Phys. J. Plus (2021) 136:516 Page 5 of 14 516

**Fig. 4** Temperature-dependent inverse magnetization for different  $\text{CrTe}_{1-x}\text{Sb}_x$  samples measured at H=0.03~T

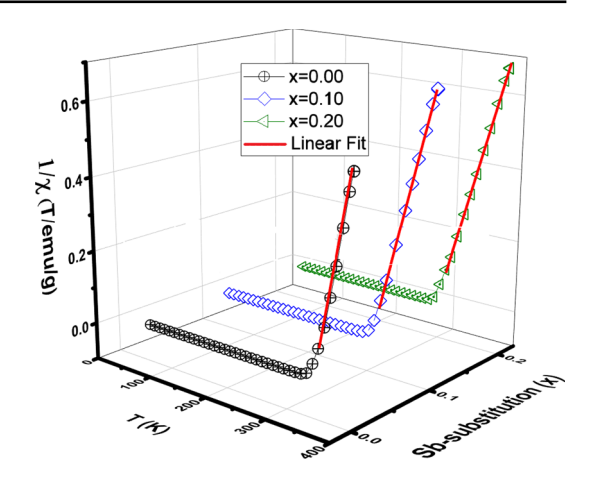
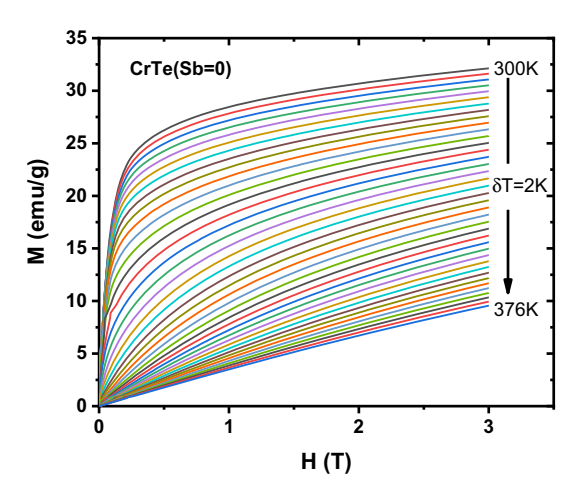


**Table 2** Effective magnetic moments and  $\theta_p$  values for the  $CrTe_{1-x}Sb_x$ 

	x = 0.00	x = 0.10	x = 0.20	
$\theta_p(K)$	342.(9)	308.(3)	301.(0)	
$\mu_{eff}(\mu_B)$	3.9(2)	4.4(0)	4.5(6)	

Fig. 5 Variations of the magnetization with field with  $\Delta T$  = 2 K intervals for CrTe sample



to investigate the critical behavior and other magnetic properties in the following sections [13, 37, 38].

### 4 Critical behaviors

The modified Arrott plots (MAP) of the magnetization along with Kouvel–Fisher (K–F) plots greatly refine the critical exponents near the phase transition [39, 40]. The K–F analysis is based on obtaining a linear behavior of the inverse the magnetic susceptibility ( $\chi_0^{-1}$ ) and the spontaneous magnetization (Ms). Moreover, Ms and  $\chi_0^{-1}$  linear graphs follow a universal



516 Page 6 of 14 Eur. Phys. J. Plus (2021) 136:516

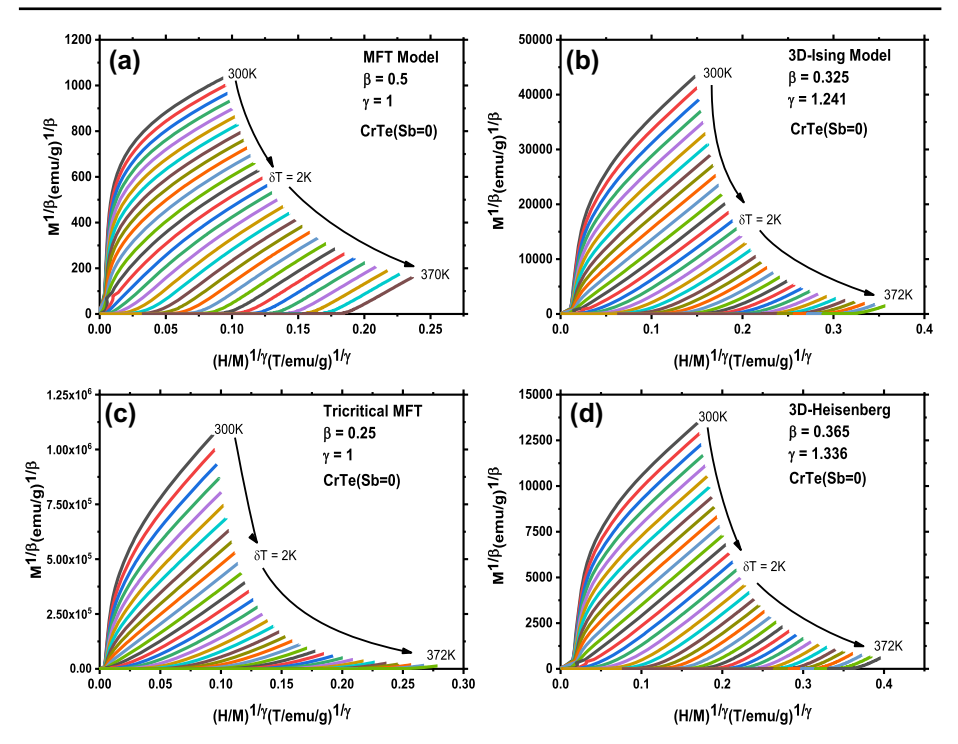


Fig. 6 Modified Arrott plots for CrTe: a mean field. b 3D-Ising. c Tricitical mean field and d 3D-Heisenberg model

behavior and their slopes determine the critical exponents [41]. Ms and  $\chi_0^{-1}$  can be obtained from:

$$M_s(T) = M_0(-\epsilon)^{\beta}, \text{below}T_c$$
 (1)

$$\chi_0^{-1} = (h_0/m_0)\epsilon^{\gamma}, \text{ above } T_c$$
 (2)

$$M = \mathrm{DH}^{1/\delta}, \ \mathrm{at}T_c$$
 (3)

where  $\beta$ ,  $\gamma$ , and  $\delta$  are the critical exponents;  $\epsilon$  is the reduced temperature; D,  $M_0$  and  $h_0/m_0$  are the critical amplitudes and M is the critical isotherm M(H) at Tc [40]. The critical exponents  $\beta$ ,  $\gamma$  take different values in different magnetic models.

According to the MAP analysis, the magnetic isotherms at high fields are expected to be parallel lines for the correct set of critical exponents. The analysis is based on Arrott–Noakes equation of state, namely:

$$(H/M)^{1/\gamma} = (T - T_C)/A + (M/B)^{1/\beta}$$
(4)

where A and B are constants [42].

The commonly used magnetic models are the tricritical mean field ( $\beta = 0.25$ ;  $\gamma = 1$ ), 3D-Heisenberg ( $\beta = 0.365$ ;  $\gamma = 1.336$ ) and the 3D-Ising ( $\beta = 0.325$ ;  $\gamma = 1.24$ ) [42].

In Fig. 6, we present the variation of  $M^{1/\beta}$  with  $(H/M)^{1/\gamma}$  for CrTe sample using various magnetic models. The initial slopes of the curves in Fig. 6 are positive above and below Tc; according to Banerjee, the positive slopes indicate a second-order phase transition [43]. The slopes at high fields in Fig. 6 can be used to obtain the relative slope (RS) analysis



Eur. Phys. J. Plus (2021) 136:516 Page 7 of 14 516

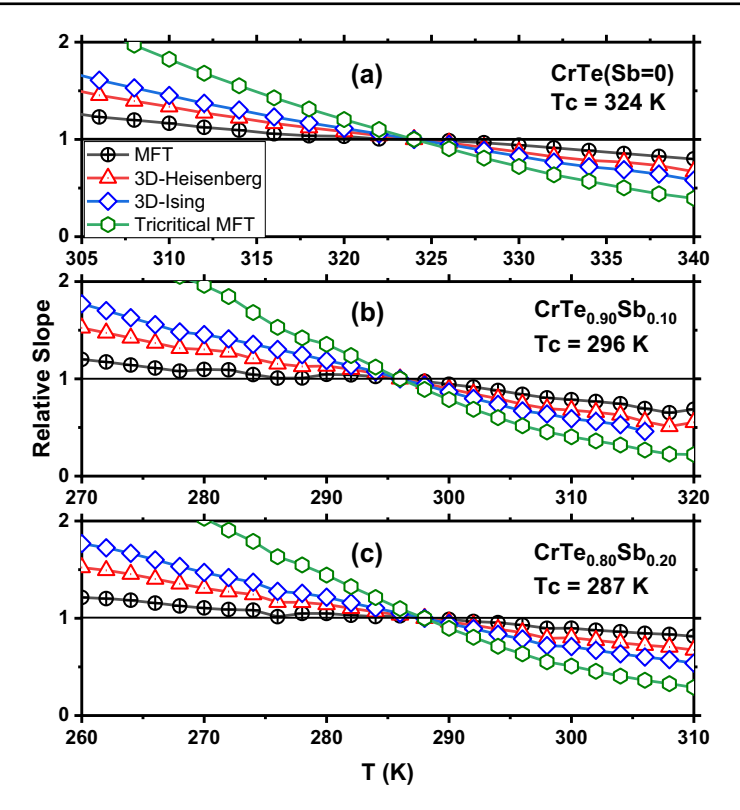


Fig. 7 Variations of the relative slope (RS) with temperature for  $CrTe_{1-x}Sb_x$ : **a** x = 0.0, b = 0.1 and **c** x = 0.2 samples

that allows us to determine the most suitable magnetic model that closely represents the magnetic isotherms. The RS values obtained from Fig. 6 are represented in Fig. 7. The RS curve obtained from mean field model is the closest to the horizontal line at RS = 1 above and below Tc indicating that the mean field model closely represents CrTe magnetic state [44]. Similar analysis has been applied for  $\text{CrTe}_{1-x}\text{Sb}_x$  samples. We found that the mean field model closely represents the magnetic isotherms in the modified Arrott plot representation. The RS curves for  $\text{CrTe}_{1-x}\text{Sb}_x$  samples are presented in Fig. 7, and the modified Arrott plots using the mean field theory (MFT) (for x = 0.10 and 0.20) are shown in Fig. 8. It is worth mentioning that, for x = 0.20, there are noticeable differences between the previously published data and results obtained in this work (see [29] for comparison). Such differences may be caused by the better quality of the samples used in the current study and the observed relaxation of the atomic bond in the (a-b)-plane especially at high Sb concentration.

The mean field representation of the modified Arrott plots (Figs. 6, 8) has been used to extract the spontaneous magnetization  $M_s(T)$  and the inverse of the magnetic susceptibility  $\chi_0^{-1}(T)$ . At each temperature, the curves at high fields are linearly fitted to Eq. 4 and extended to the  $M^{I/\beta}$  and  $(H/M)^{I/\gamma}$  axes. The intercept points represent the  $M_s(T)$  and  $\chi_0^{-1}$ . The variations of  $M_s(T)$  and  $\chi_0^{-1}(T)$  with temperature for  $CrTe_{1-x}Sb_x$  samples with x=0.0,0.1 and 0.2 are presented in Figs. 9a, 10a and 11a, respectively, and then fitted to Eqs. 1 and 2 in order to evaluate the critical exponents  $\beta$  and  $\gamma$  along with the transition temperature Tc. The obtained values for CrTe sample are:  $\beta=0.49\pm0.10$ ,  $and\gamma=1.04\pm0.02$  and



516 Page 8 of 14 Eur. Phys. J. Plus (2021) 136:516

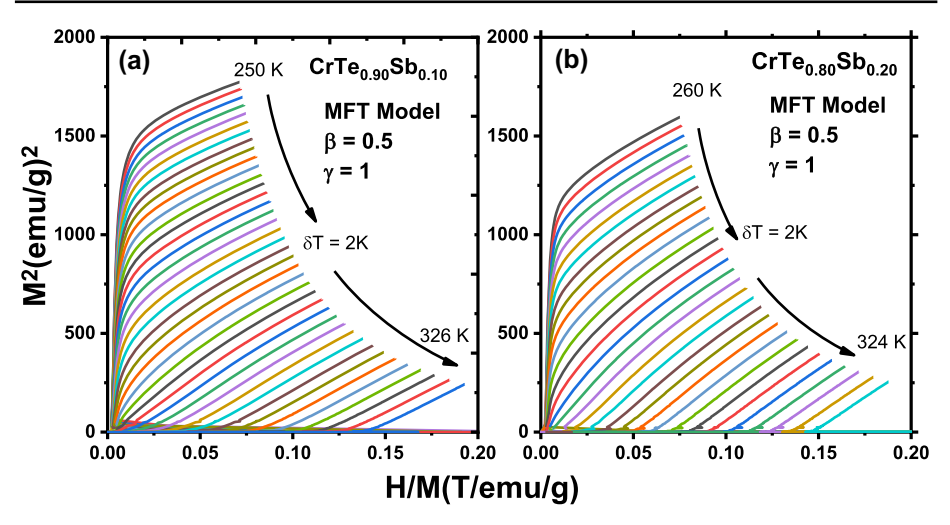


**Fig. 8** Modified Arrott plots using MFT for  $CrTe_{1-x}Sb_x$  (x = 0.1 and 0.2)

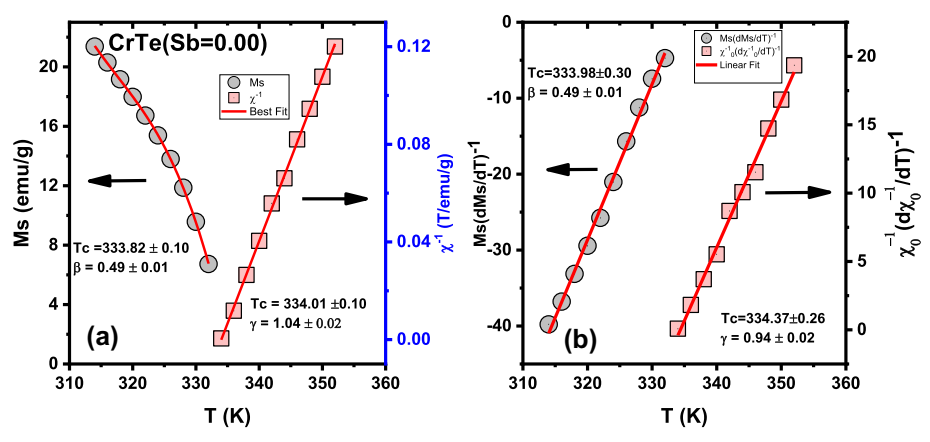


**Fig. 9 a** Variations of Ms and  $\chi_0^{-1}$  with temperature, **b** Kouvel–Fisher plots for Ms(T) and  $\chi_0^{-1}$ (T) plot for CrTe

Tc = 334.0  $\pm$  0.1. Similarly, for CrTe<sub>1-x</sub>Sb<sub>x</sub> with x = 0.1 and 0.2, the values are: ( $\beta$  =  $0.50 \pm 0.01$ ,  $\gamma = 0.99 \pm 0.01$  and  $Tc = 303.3 \pm 0.1$ ) and  $(\beta = 0.51 \pm 0.01, \gamma = 1.00 \pm 0.01)$ and  $Tc = 295.4 \pm 0.1$ ), respectively.

The Kouvel-Fisher (K-F) plots representations of the spontaneous magnetization and the susceptibility greatly improve the accuracy of modified Arrott analysis for the critical exponents. According to the (K–F) model [40],

$$\frac{M_s(T)}{\mathrm{d}M_s(T)/\mathrm{d}T} = \frac{T - T_c}{\beta} \tag{5}$$

$$\frac{M_s(T)}{dM_s(T)/dT} = \frac{T - T_c}{\beta}$$

$$\frac{\chi_0^{-1}(T)}{d\chi_0^{-1}(T)/dT} = \frac{T - T_c}{\gamma}$$
(6)

Both equations are linear in temperature (T-Tc) with slopes equal to  $1/\beta$  and  $1/\gamma$ . Figures 9b, 10b and 11b illustrate the K-F plot for  $CrTe_{1-x}Sb_x$  samples with x = 0.0, 0.1 and



Eur. Phys. J. Plus (2021) 136:516 Page 9 of 14 516

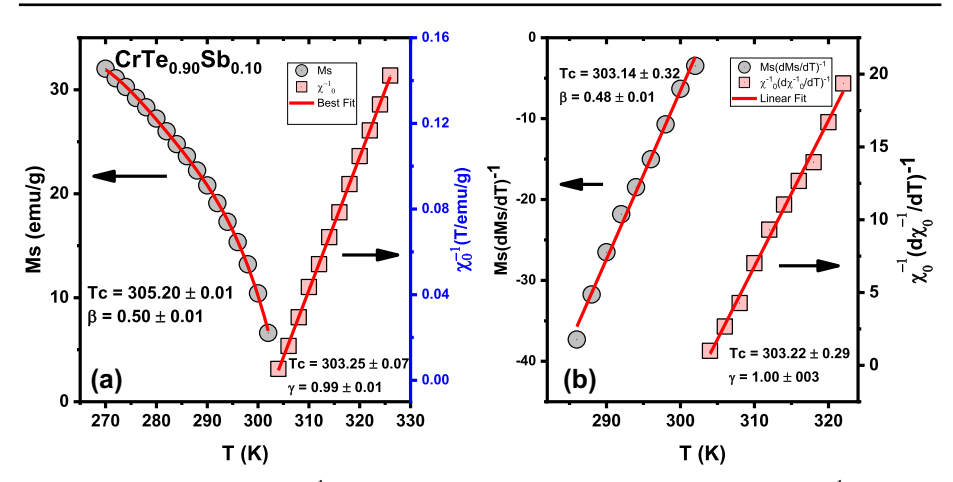


Fig. 10 a Variations of Ms and  $\chi_0^{-1}$  with temperature, b Kouvel–Fisher plots for Ms(T) and  $\chi_0^{-1}$ (T) plot for  $CrTe_{0.9}Sb_{0.1}$ 

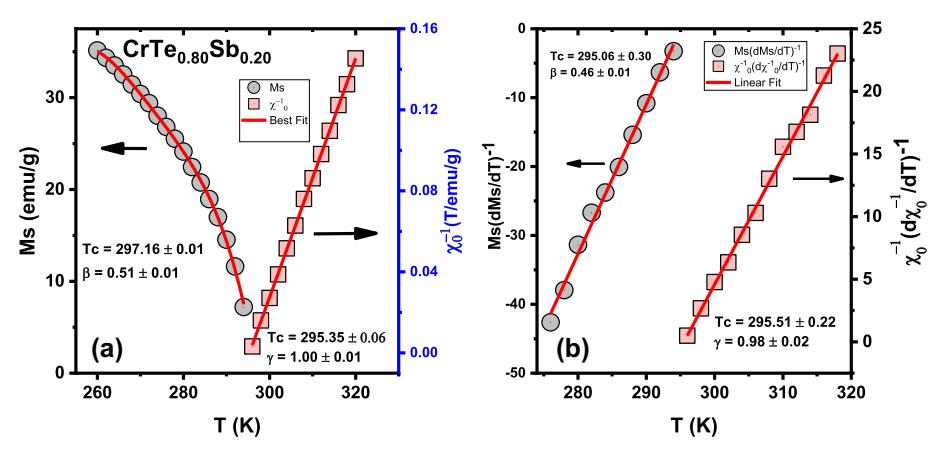


Fig. 11 a Variations of Ms and  $\chi_0^{-1}$  with temperature, b Kouvel–Fisher plots for Ms(T) and  $\chi_0^{-1}$ (T) plot for  $CrTe_{0.8}Sb_{0.2}$ 

0.2, respectively. The obtained critical exponents for x=0.0 are:  $\beta=0.49\pm0.01$  and  $\gamma=0.94\pm0.02$  with Tc = 334.4±0.3 K. We notice that  $\beta$  is very close to the values obtained using the modified Arrott plot while  $\gamma$ -value has been slightly reduced but still near the theoretical mean field value. Similar results have been obtained for x=0.10 and x=0.20, which are shown in Figs. 10b and 11b. All values of the critical exponents extracted from MAP as well as K–F are given in Table 3. Moreover, to obtain more accurate critical exponents ( $\beta$ , and  $\gamma$ ) and the critical temperature Tc, we have adopted the iterative method for the unsubstituted sample (CrTe) based on K–F method (Eqs. 5 and 6). The results shows, after four rounds, that the values of the critical exponents with Tc are stable and close to the standard mean field model, namely  $\beta=0.5$ , and  $\gamma=1$ , within the uncertainty (see Table 4).

The values of third critical exponent  $(\delta)$  can be calculated using the Widom scaling relation:  $\delta = 1 + \frac{\gamma}{\beta}$ , and  $\beta$  and  $\gamma$  values obtained from MAP and K–F method [45]. The values are listed in Table 3.



516 Page 10 of 14 Eur. Phys. J. Plus (2021) 136:516

Table 3	Critical ext	ponents along	with Tc	for CrTe1	-xSbx ((	0.0 < x < 0.0	< 0.2) sa	mples

Sample	Model	Tc (K)	β	γ	δ Theory	δ expt
CrTe	MAP	$334.0 \pm 0.1$	$0.49 \pm 0.01$	$1.04 \pm 0.02$	$3.12 \pm 0.12$	$2.95 \pm 0.01$
	K-F	$334.4 \pm 0.3$	$0.49 \pm 0.01$	$0.94 \pm 0.02$	$2.92\pm0.12$	
CrTe <sub>0.90</sub> Sb <sub>0.10</sub>	MAP	$303.3 \pm 0.1$	$0.50\pm0.01$	$0.99 \pm 0.01$	$2.98\pm0.09$	$3.11\pm0.01$
	K-F	$303.2 \pm 0.3$	$0.48\pm0.01$	$1.00 \pm 0.03$	$3.08 \pm 0.16$	
$CrTe_{0.80}Sb_{0.20}$	MAP	$295.4 \pm 0.1$	$0.51\pm0.01$	$1.00\pm0.01$	$2.96 \pm 0.09$	$2.90\pm0.01$
	K-F	$295.5 \pm 0.2$	$0.46\pm0.01$	$0.98\pm0.02$	$3.13 \pm 0.13$	

**Table 4** Critical exponents along with Tc for CrTe sample using the iterative method

Iteration #	Initials		Tc (K)	β	γ
	β	γ			
0	0.5	1	$334.37 \pm 0.26$	$0.49 \pm 0.01$	$0.94 \pm 0.02$
1	0.49	0.94	$334.63 \pm 0.52$	$0.48\pm0.01$	$0.96 \pm 0.03$
2	0.48	0.96	$333.95 \pm 0.53$	$0.48\pm0.01$	$0.97\pm0.03$
3	0.48	0.97	$333.75 \pm 0.54$	$0.48\pm0.01$	$0.98\pm0.03$

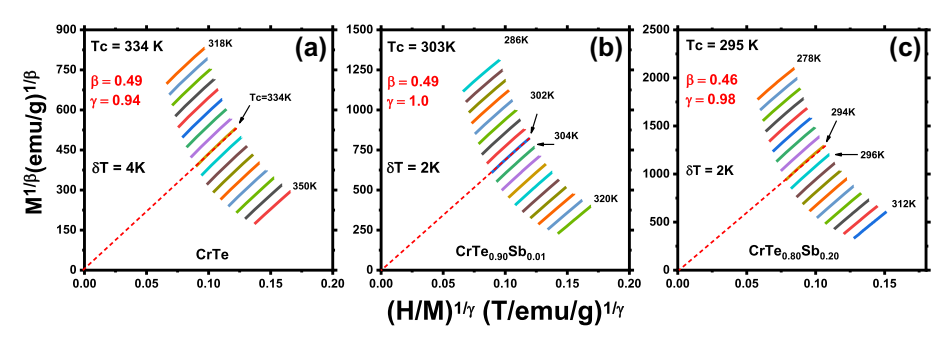


Fig. 12 Modified Arrott plot of  $M^{1/\beta}$  versus  $(H/M)^{1/\gamma}$  at high field values with the obtained critical exponents of  $\beta$  and  $\gamma$  with a red linear dashed curve passed through the origin for. a CrTe, b CrTe<sub>0.90</sub>Sb<sub>0.10</sub>, and c CrTe<sub>0.80</sub>Sb<sub>0.20</sub>

To illustrate the validity of the K–F analysis and the confidence in the obtained critical exponents and critical behavior, we used these critical exponents to replot the modified Arrott plots in Fig. 12. The figure shows a set of nearly perfect parallel straight lines at high field (H > 2 T), indicating that the critical exponents  $\beta$  and  $\gamma$  values obtained using K–F method for the mean field model are quite accurate choice. Moreover, the dashed lines in Fig. 12 are a linear fitting of isothermal magnetization extrapolated near to the origin point (0,0). The obtained Tc values are 334 K, 302 K and 294 K for x = 0, 0.1 and 0.2, respectively. These values are in agreement with the Tc values obtained from K–F analysis. This further indicates that the critical exponents are close agreement with the MFT critical exponents.

Equation 3 should yield a linear graph of the magnetic isotherms at (T = Tc) in a log-log presentation (Fig. 13) with a slope =  $1/\delta$ . The linear fit yields  $\delta = 2.95 \pm 0.01$ . The result is consistent with the one obtained from Widom's relation as shown in Table 3.



Eur. Phys. J. Plus (2021) 136:516 Page 11 of 14 516

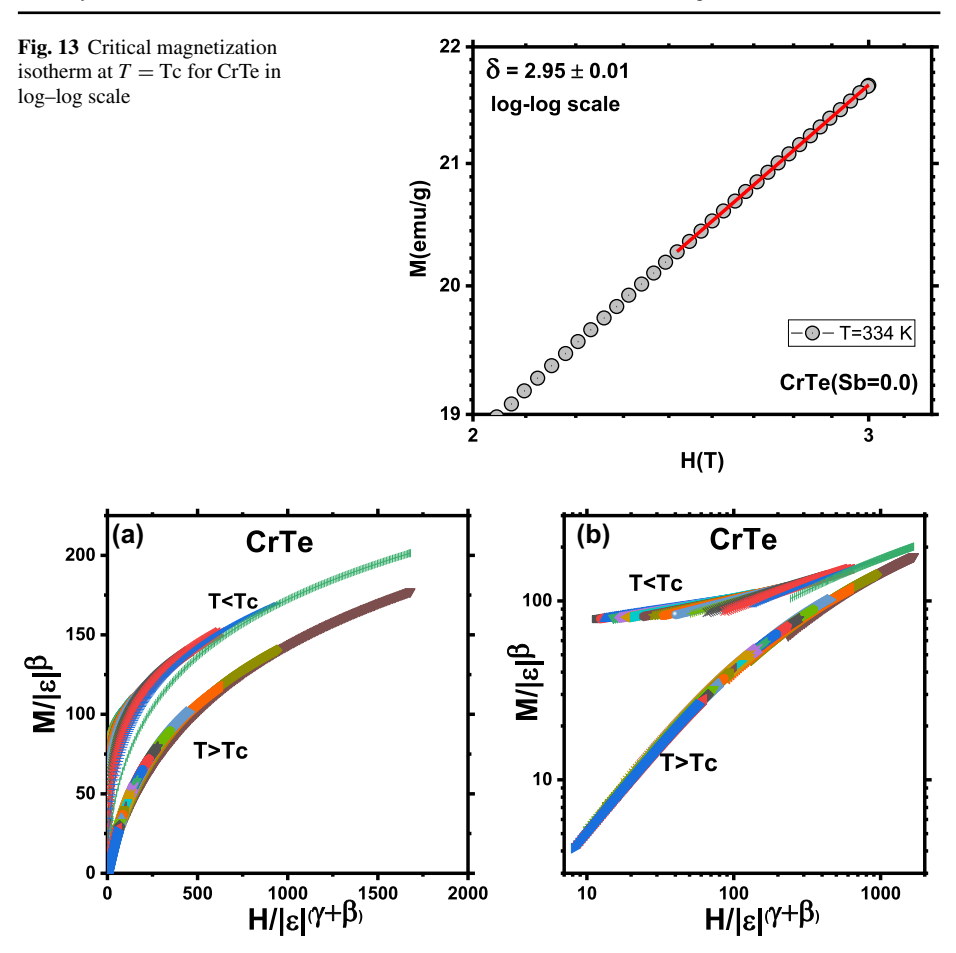


Fig. 14 a Universal scaling behavior above and below Tc for CrTe. b log-log scale representation

Close to the transition temperature Tc, the normalized equation of state can be expressed as:

$$m = f_{+}(h) \tag{7}$$

where  $f_{\pm}$  are functions above (+) and below (-) Tc;  $m \equiv |\varepsilon|^{-\beta} M(H, \varepsilon)$  is the normalized magnetization and  $h \equiv H|\varepsilon|^{-(\beta+\gamma)}$  is the normalized field.

For the correct values of the critical exponents, Eq. (7) implies that for the reliable values of  $\beta$ ,  $\gamma$  and  $\delta$ ; two universal branches above and below Tc presented as  $M/|\varepsilon|^{\beta}$  vs.  $H/|\varepsilon|^{(\beta+\gamma)}$  [44]. Both curves merge asymptotically at  $T=\mathrm{Tc}$ . The critical exponents  $(\beta,\gamma)$  and  $\delta$ 0 obtained from Kouvel–Fisher analysis are used to represent the normalized magnetization isotherm (m) versus the normalized field (h) for all investigated samples. The scaled data for CrTe sample are presented in Fig. 14 as two branches of the magnetization above and below Tc. At high fields, both branches are converging toward each other at Tc. Figure 14b shows the data in log–log scale, which vividly reveals the merge of the data giving further evidence for the reliability of the critical exponents' values within the mean field model. The scaling analysis has been applied for  $\mathrm{CrTe}_{1-x}\mathrm{Sb}_x$  for x=0.10 and x=0.20. The results are shown in



516 Page 12 of 14 Eur. Phys. J. Plus (2021) 136:516

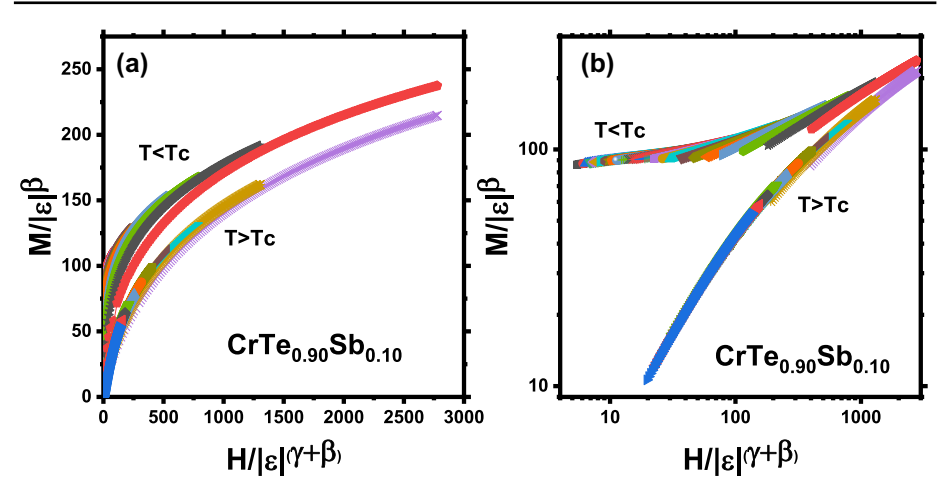


Fig. 15 a Universal scaling behavior above and below Tc for CrTe<sub>0.90</sub>Sb<sub>0.10</sub>. b log-log scale representation

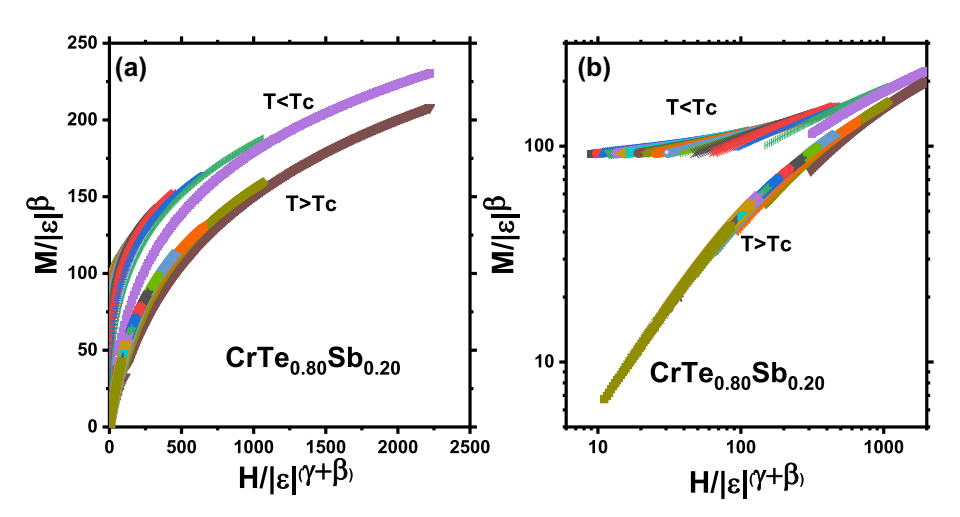


Fig. 16 a Universal scaling behavior above and below Tc for CrTe<sub>0.80</sub>Sb<sub>0.20</sub>. b log-log scale representation

Figs. 15 and 16, respectively. The well-scaled data for x = 0.20 in the current work comparing to the scaled data published in [29] further confirm the differences and improvements in the experiment conditions.

#### 4.1 Conclusion

We investigated the structural and critical behavior of  $\text{CrTe}_{1-x}\text{Sb}_x$  with varying Sb contents. Antimony substitution resulted in pure NiAs-hexagonal structure with P6<sub>3</sub>/mmc (194) space group. The critical exponents ( $\beta$ ,  $\gamma$ , and  $\delta$ ) follow mean field model for all samples with different Sb concentrations. The magnetization isotherms near the ferromagnetic transition follow a universal scaling behavior, giving further support for the mean field behavior in  $\text{CrTe}_{1-x}\text{Sb}_x$  and confirming the obtained values of the critical exponents.



Eur. Phys. J. Plus (2021) 136:516 Page 13 of 14 516

**Acknowledgements** Authors from KFUPM acknowledge the support provided by the Deanship of Scientific Research at King Fahd University of Petroleum and Minerals (KFUPM) for funding this work under project No. SR191008. AAE acknowledges the start-up and rising stars funds by UTEP and UT-system, respectively, and the partial support by the US National Science Foundation under award No. 2009358.

#### References

- F. Lotgering, E. Gorter, Solid solutions between ferromagnetic and antiferromagnetic compounds with NiAs structure. J. Phys. Chem. Solids 3, 238–249 (1957). https://doi.org/10.1016/0022-3697(57)90028-8
- M. Venkatraman, J. Neumann, The Cr-Sb (Chromium-Antimony) system. J. Phase Equilib. (1990). https://doi.org/10.1007/bf02898255
- H. Okamoto, Cr-Sb (chromium-antimony). J. Phase Equilib. 13, 438–439 (1992). https://doi.org/10.100 7/bf02674996
- H. Ipser, K. Komarek, K. Klepp, Transition metal-chalcogen systems viii: The Cr-Te phase diagram. J. Less Common Metals. 92, 265–282 (1983). https://doi.org/10.1016/0022-5088(83)90493-9
- H. Haraldsen, A. Neuber, Magnetochemische Untersuchungen. XXVII. Magnetische und röntgenographische Untersuchungen am System Chrom-Tellur. Zeitschrift Für Anorganische Und Allgemeine Chemie. 234, 353–371 (1937). https://doi.org/10.1002/zaac.19372340407
- 6. O. Beckman and L. Lundgren, Handbook of Magnetic Materials (1991).
- M. Akram, F. Nazar, Magnetic properties of CrTe, Cr23Te24, Cr7Te8, Cr5Te6, and Cr3Te4 compounds.
   J. Mater. Sci. 18, 423–429 (1983). https://doi.org/10.1007/bf00560631
- G. Street, E. Sawatzky, K. Lee, Magnetic properties of vapor grown crystals of hexagonal chromium telluride. J. Phys. Chem. Solids 34, 1453–1455 (1973). https://doi.org/10.1016/s0022-3697(73)80048-4
- M. McGuire, V. Garlea, S. KC, V. Cooper, J. Yan, H. Cao, et al., Antiferromagnetism in the van der Waals layered spin-lozenge semiconductor CrTe3. Phys. Rev. B (2017). https://doi.org/10.1103/physrevb.95.14 4421
- N. Grazhdankina, Magnetic first order phase transitions. Soviet Phys. Uspekhi. 11, 727–745 (1969). https://doi.org/10.1070/pu1969v011n05abeh003744
- S. Polesya, G. Kuhn, D. Benea, S. Mankovsky, H. Ebert, Electronic structure and magnetic properties of chromium chalcogenides and pnictides with NiAs structure. Z. Anorg. Allg. Chem. 639, 2826–2835 (2013). https://doi.org/10.1002/zaac.201300314
- B. Chittari, Y. Park, D. Lee, M. Han, A. MacDonald, E. Hwang et al., Electronic and magnetic properties of single-layer MPX<sub>3</sub> metal phosphorous trichalcogenides. Rev. B Phys (2016). https://doi.org/10.1103/ physrevb.94.184428
- P. Ajayan, P. Kim, K. Banerjee, Two-dimensional van der Waals materials. Phys. Today 69, 38–44 (2016). https://doi.org/10.1063/pt.3.3297
- M. Hamad, E. Martinez-Teran, Y. Maswadeh, R. Hamad, E. Al-Nahari, A. El-Gendy et al., Room temperature magnetocaloric effect in CrTe1-xSbx alloys. J. Magn. Magn. Mater. 514, 167171 (2020). https://doi.org/10.1016/j.jmmm.2020.167171
- L. Zhang, X. He, A. Zhang, Q. Xiao, W. Lu, F. Chen et al., Tunable Curie temperature in layered ferromagnetic Cr<sub>5+x</sub>Te<sub>8</sub> single crystals. APL Mater. 8, 031101 (2020). https://doi.org/10.1063/1.514338
- A. Andresen, E. Zeppezauer, T. Boive, B. Nordström, C. Brändén, The magnetic structure of Cr2Te3, Cr3Te4, and Cr5Te6. Acta Chem. Scand. 24, 3495–3509 (1970). https://doi.org/10.3891/acta.chem.scand. 24-3495
- M. Chevreton, E. Bertaut, F. Jellinek, Quelques remarques sur le système Cr–Te. Acta Crystallogr. A 16, 431–431 (1963). https://doi.org/10.1107/s0365110x63001134
- 18. J.B. Goodenough, Magnetism and the Chemical Bond (Interscience, New York, 1963).
- G. Bhimanapati, Z. Lin, V. Meunier, Y. Jung, J. Cha, S. Das et al., Recent advances in two-dimensional materials beyond graphene. ACS Nano 9, 11509–11539 (2015). https://doi.org/10.1021/acsnano.5b0555
- N. Suzuki, T. Kanomata, R. Konno, T. Kaneko, H. Yamauchi, K. Koyama et al., Magnetic phase diagram of CrTe1−xSbx (0.0≤x≤1.0). J. Alloys Compd. 290, 25–29 (1999). https://doi.org/10.1016/s0925-8388 (99)00244-3
- T. Hirone, S. Maeda, I. Tsubokawa, N. Tsuya, On the magnetic properties of the system MnSb–CrSb. J. Phys. Soc. Jpn. 11, 1083–1087 (1956). https://doi.org/10.1143/jpsj.11.1083



516 Page 14 of 14 Eur. Phys. J. Plus (2021) 136:516

 A. Snow, Magnetic Moment Orientation and Thermal Expansion of Antiferromagnetic CrSb. Rev. Mod. Phys. 25, 127–127 (1953). https://doi.org/10.1103/revmodphys.25.127

- A. Snow, Neutron diffraction investigation of the atomic magnetic moment orientation in the antiferromagnetic compound CrSb. Phys. Rev. 85, 365–365 (1952). https://doi.org/10.1103/physrev.85.365
- W. Takei, D. Cox, G. Shirane, Magnetic structures in the MnSb-CrSb system. Phys. Rev. 129, 2008–2018 (1963). https://doi.org/10.1103/physrev.129.2008
- N.P. Grazhdankina, L.G. Gaidukov, K.P. Rodionov, M.I. Oleinik, V.A. Shchipanov, J. Exptl. Theoret. Phys. (U.S.S.R.) 40, 433–440 (1961)
- W. Takei, D. Cox, G. Shirane, Magnetic structures in CrTe—CrSb solid solutions. J. Appl. Phys. 37, 973–974 (1966). https://doi.org/10.1063/1.1708545
- Grazhdankina N P and Zaynullina R I, Zh. Eksp. Teor. Fiz. 59 1896 (1970) (Engl. Trans. Sou. Phys.-JETP 32 1025 (1971)).
- P. de Gennes, Effects of Double Exchange in Magnetic Crystals. Phys. Rev. 118, 141–154 (1960). https://doi.org/10.1103/physrev.118.141
- M. Hamad, K. Ziq, Critical behavior of CrTe1-xSbx ferromagnet. AIP Adv. 8, 101416 (2018). https://doi.org/10.1063/1.5042550
- A. West, Solid State Chemistry and Its Applications, 2nd edn. (Wiley, Chichester, West Sussex, , 2014), p. 187
- M. Hamad, I. Abdel-Latif, K. Ziq, Effect of cobalt doping in Nd1-xSrxMn1-yCoyO3. J. Phys: Conf. Ser. 869, 012032 (2017). https://doi.org/10.1088/1742-6596/869/1/012032
- L. Elton, D. Jackson, X-Ray Diffraction and the Bragg Law. Am. J. Phys. 34, 1036–1038 (1966). https://doi.org/10.1119/1.1972439
- H. Rietveld, The Rietveld method. Phys. Scr. 89, 098002 (2014). https://doi.org/10.1088/0031-8949/89/9/098002
- K. El-Sayed, Z. Heiba, Quantitative phase analysis from X-ray powder diffraction data using a two-stage method. Powder Diffr. 9, 246–249 (1994). https://doi.org/10.1017/s0885715600018959
- H. Harladsen, Die Phasenverhältnisse im system chrom-schwefel. Z. Anorg. Allg. Chem. 234, 372–390 (1937). https://doi.org/10.1002/zaac.19372340408
- T. Kong, K. Stolze, D. Ni, S. Kushwaha, R. Cava, Anisotropic magnetic properties of the ferromagnetic semiconductor CrSbSe3. Phys. Rev. Mater. (2018). https://doi.org/10.1103/physrevmaterials.2.014410
- M. Hamad, PhD thesis, "Developing Near Room Temperature Magnetocaloric Materials", King Fahd University of Petroleum and Minerals, (2018). http://eprints.kfupm.edu.sa/140778/
- 38. M. Hamad, Y. Maswadeh, K. Ziq, Effects of Ni substitutions on the critical behaviors in Nd0.6Sr0.4Mn1-xNixO3 manganite. Journal of Magnetism And Magnetic Materials. **491**, 165609 (2019). https://doi.org/10.1016/j.jmmm.2019.165609
- A. Arrott, Criterion for ferromagnetism from observations of magnetic isotherms. Phys. Rev. 108, 1394–1396 (1957). https://doi.org/10.1103/physrev.108.1394
- J. Kouvel, M. Fisher, Detailed magnetic behavior of nickel near its curie point. Phys. Rev. 136, A1626–A1632 (1964). https://doi.org/10.1103/physrev.136.a1626
- H. Stanley, Introduction to phase transitions and critical phenomena (Oxford Univ. Press, New York, 1987). https://doi.org/10.1002/qua.560350412.
- A. Arrott, J. Noakes, Approximate equation of state for nickel near its critical temperature. Phys. Rev. Lett. 19, 786–789 (1967). https://doi.org/10.1103/physrevlett.19.786
- B. Banerjee, On a generalised approach to first and second order magnetic transitions. Phys. Lett. 12, 16–17 (1964). https://doi.org/10.1016/0031-9163(64)91158-8
- J. Fan, L. Ling, B. Hong, L. Zhang, L. Pi, Y. Zhang, Critical properties of the perovskite manganiteLa0.1Nd0.6Sr0.3MnO3. Phys. Rev. B (2010). https://doi.org/10.1103/physrevb.81.144426
- B. Widom, Degree of the critical isotherm. J. Chem. Phys. 41, 1633–1634 (1964). https://doi.org/10.106 3/1.1726135

